Egypt.J.Chem. **Vol. 62**, Special Issue (Part 1), pp. 327 - 346 (2019)

Egyptian Journal of Chemistry
http://ejchem.journals.ekb.eg/

Terahertz Pulsed Spectroscopy for Optical and Dielectric Properties of Demineralized Bone Matrix, Collagen and Hydroxyapatite

S. K. H. Khalil[1*], W. M. El hotaby[1], G. T. El-Bassyouni[2]

[1]Spectroscopy Department, Physics Division, National Research Centre (NRC), Dokki, Giza, 12622, Egypt,

[2]Refractories, Ceramics and Building Materials Department, Inorganic Chemical Industries and Mineral Resources Division, National Research Centre (NRC), Dokki, Giza, 12622, Egypt.

DEMINERALIZED bone matrix (DBM) has osteoinductive potential functioning in many biological applications such as three-dimensional scaffold which assist new bone and cartilage growth by enhanced bioavailability of growth factors. Terahertz pulsed spectroscopy (TPS) was applied to investigate the optical and dielectric properties of camel femoral and cranial DBM, collagen type I, synthetic and natural hydroxyapatite powder (HA) in the range of 0.06-3.5THz. Terahertz (THz) absorption, refractive index (R.I) and dielectric properties (ε′ and ε″) were found to be intensely differentiated to control and demineralized bone. Results presented the THz absorption fingerprint of all studied materials. The natural HA revealed higher R.I, ε′, and ε″ values than both synthetic HA and collagen. Cranial DBM exhibited higher R.I compared to the control in all frequency ranges, whereas the femoral DBM behavior was frequency dependent. Demineralization produced significant increase in the values of ε′ and ε″. THz dielectric properties acted as a sensitive predictor to the composition and microstructure of bone in different biological applications. Amalgamation of Infrared Spectroscopy and THz spectroscopy together with TGA, ICP and EDX can offer deep insight into the sample properties.

Keywords: Demineralized bone, Collagen, Terahertz Spectroscopy, Refractive Index, Dielectric properties

Introduction

Bone matrix is the extracellular component of bone. It is composed of an organic phase recognized as osteoid (35%) [mainly made up of type I collagen fibers with smaller amounts of glycosaminoglycan and other proteins] and inorganic mineral particles (65%) of carbonated hydroxyapatite (cHA) nanoparticles [1]. An essential indicator of bone mechanical properties and bone material quality is the amount of mineral incorporated into the bone [2]. The cause of the variable mineral content in bone is a bio-mineralization process in cooperation with the bone remodeling renewal process [3]. The spectral differences between HA and the bone mineral phases can be correlated to the chemical differences, as the mineral phase in bone is known to diverge from the crystalline hydroxyapatite by carbonization.

Demineralized bone matrix (DBM) is a more biologically active allograft that has the inorganic mineral detached, leaving behind the organic "collagen" matrix. The removal of the bone mineral reveals more biologically active bone morphogenetic proteins (BMPs) [4]. These growth factors control the differentiation of progenitor cells into osteoprogenitor ones, which control bone and cartilage formation [5]we have explored its utility in healing large osseous defects. Healing is achieved by the insertion of muscle fragments transduced with adenovirus encoding BMP-2 (Ad.BMP-2. Typically for the in vitro demineralization of bone, 0.6M

*Corresponding author e-mail: safaakhk@yahoo.com; Phone number: (+2) 01016828028

Orcid ID: 0000-0002-0588-3266
Received 1/7/2019; Accepted 5/8/2019
DOI: 10.21608/ejchem.2019.14201.1876

hydrochloric acid (HCl) was used to resolve the mineral phase, leaving the organic phase virtually intact [6]however, it has not been used to study the OH-band in bone. A sequential dehydration protocol was developed to replace unbound (heat drying. Collagen type-1, is the most abundant load-bearing protein which makes up 90-95% of the organic matrix. The principal extracellular matrix (ECM) components of both subchondral bone and hyaline cartilage are collagen type 1 and 2, they influenced cell morphology, cell adhesion and biosynthetic activity [7].

Vibrational spectroscopic techniques such as Fourier transform Raman and Infrared Spectroscopy FT-IR are suitable for characterizing the organic and inorganic constituents of bone. Collagen destabilization produced by weak forces are hard to be detected by symmetric or high-energy vibrations due to the small spectral changes [8]. Far-infrared spectroscopy (F-IR) covers the electromagnetic spectrum range from 50-500cm^{-1}. To some extent it overlaps with the Terahertz spectroscopy restricted to the range 0.3-3THz (10-100cm^{-1}) [9].

In the region between the IR and microwave of the electromagnetic spectrum, the THz radiation occupies the frequency range of 0.1–10THz [10]which lies within the frequency range of 0.1–10 THz. They represent a large portion of the electromagnetic spectrum and have wide application potentials. THz radiation can penetrate into thin layers of nonmetallic substances like clothing, plastic, and ceramics up to several millimeters. Radiographic imaging using X-rays has been the primary diagnostic imaging technology used within the dental profession since its discovery in 1895. However, it is an ionising radiation with some detrimental effects to our healthand has inherent limitations, such as; superimposition of anatomical structures and poor soft tissue contrast [1]. Unlike X rays, Terahertz waves are non-ionizing and therefore they do not pose a risk to living organisms. Also, they provide images that are comparable to backscatter X-rays. This technology can be used for security screening, semiconductor inspection, food inspection, pharmaceutical inspection, and 2D and 3D imaging, including medical diagnosis in the areas of tooth structure, skin cancer and tumors [1,2]. Both terahertz pulsed spectroscopy (TPS. THz with the privilege of being non-ionizing radiation has comprehensive applications. Theoretical and experimental studies demonstrated that many intramolecular, and intermolecular vibrational modes of biological macromolecules like hydrogen bonds, Van der Waals forces, dipole rotational and vibrational transitions correspond to the low frequency band of THz (0.1-3 THz) [11], thus provide a unique fingerprint of the molecular structure. Owing to the lower Doppler effects, THz spectroscopy has better resolution than the IR spectroscopy [12,13] bovine serum albumin and collagen in the 0.06-2.00 THz (2-67 cm(-1.

Recently, Terahertz time-domain spectroscopy (THz-TDS) has been used to study the spectroscopic properties of numerous materials in the spectral region of 0.1-3THz [14,15] and obtain the THz optical parameters, refractive index and absorption coefficient spectra, to probe the intermolecular interactions [16]. Terahertz pulsed spectroscopy (TPS) is recommended for measuring absorption down to 2 cm^{-1}, and low-frequency spectral analysis over FT-IR because its sample preparation and data acquisition remove etalon effects and its signal/noise ratio is of 10000:1[12]. Hence, it is commendable to study the structure, composition and the interaction mechanisms on the basis of the material characteristic response to the THz radiation [17]. TPS is a direct field measurement, it allows the complex dielectric function to be measured without more fitting routine [12]. The accurate terahertz (THz) electrical and optical properties of biomaterials are essential as the biological applications of the THz electromagnetic waves are recently growing [18]. The current study is planned to assess the potential use of TPS to obtain new insight into the structure and chemical composition of the demineralized bone matrix (DBM), collagen and hydroxyapatite in regard to their optical and dielectric properties.

Materials and Methods

Synthetic hydroxyapatite (calcium phosphate hydroxide, Lot # 73H7180) and collagen type I from calf skin (C9791) were purchased from Sigma-Aldrich.

Demineralized matrices

Camel femur and cranial bones were obtained from healthy mature sacrificed animals. The proximal and distal ends of femur bones were resected. Muscles, periosteum and adherent soft tissues were mechanically removed using a scalpel. Bones were scrubbed using a stiff brush and bone marrow was discarded. The diaphysis

were cut longitudinally into small slabs while, the cranial bone were cut into segments via a bone cutter. Both slabs and segments were washed with copious amount of distilled water for 2 hours. Then dehydrated using absolute ethanol followed by ethyl ether in order to remove cellular, potentially antigenic materials and lipids. Bone samples were allowed to dry overnight at room temperature. Demineralization process was obtained by immersion in 0.6M HCl for 24 hours while stirring at room temperature. The ratio of demineralizing solution and bone weight in grams was always kept constant at 25ml/gram of bone. At the end of the demineralization process bones were washed using distilled water to remove any attached salts then dried at room temperature for 24 hours to retain transforming potency [19].

Natural Hydroxyapatite Powder (Cortex)

Natural hydroxyapatite powder was obtained from the cortex of freshly removed diaphysis of the calf long bones. Bones were dissected of the connective tissues and alkali treated by boiling for 4h in 30% $NaCO_3$ solution, washed thoroughly with hot distilled water, then dried at 100^{o}C overnight. The cycle of alkali treatment was repeated to reach constant weight of the sample. Deproteinated bones were ground and sieved to obtain suitable particle size of 90-125µm [20,21]

Instruments

TPS spectra 3000 spectrometer (Teraview Ltd., Cambridge, UK) was used for THz absorption and permittivity measurements in transmission mode, where 10% sample concentration in 400 mg polyethylene disc was prepared. THz properties were recorded by averaging three-measured samples. The Boltzmann fitting model was used to fits the experimental results of the real and imaginary parts of the dielectric properties well within the measured spectral range of 0.06-2.5THz, where the signal-to-noise ratio is considerably good using origin lab software (Origin Lab Corporation, Northampton, MA) for the refractive index (R.I) and the dielectric properties.

All materials under investigation were analyzed by Bruker Optics Vertex 70 FT-IR spectrometer (Germany). All powder samples were prepared in the form of 1% concentration in 200 mg KBr discs for collecting the FT-IR spectra. Collagen's spectra were collected in the reflection mode using attenuated total reflection unit (ATR-diamond crystal) due to its fibrous nature. All specimens' measurements were performed on three samples at room temperature (20±1C^{0}).

The thermogravemetric analysis (TGA) of the samples was performed by accurately weighing samples then heating with a rate of 10C^{o}/ minute up to 1000C^{o} using a Shimadzu TGA-50 thermal analyzer- Japan. In order to calculate the percentage degree of demineralization, the loss in weight accompanying thermal changes recorded as a function of temperature was detected ending up with the ash content.

$$\%D.D=(w_c-w_t/w_c)\times 100$$

Where, w_c and w_t are the ash weight of the control and treated bones, respectively.

In order to quantify the Ca and P contents in samples under investigation, Agilent 5100 Inductively Coupled Plasma – Optical Emission Spectrometer (ICP-OES) with Synchronous Vertical Dual View (SVDV) was used. All samples were digested using nitric acid, where it is an acceptable matrix for consistent recovery of metals which are compatible with the analytical method *(APHA, 2015)*. For each series of measurements intensity calibration curve was constructed composed of a blank and three or more standards from Merck company (Germany). Accuracy and precision of the metals measurements were confirmed using external reference standards from Merck.

Samples were examined for morphological changes and elemental distribution by scanning electron microscopy (SEM)/ energy-dispersive X-ray spectroscopy (EDX) in a SEM Model Quanta FEG 250, Holland.

Results and Discussion

THz Optical Properties

Absorption spectra

Several materials and tissues have "terahertz signatures". Different types of bone tissue were characterized according to their THz response measured using the TPS. The THz absorbance spectra of both inorganic constituent (cortex powder) and major organic constituent (collagen type I) are illustrated in Figure 1(i). THz absorption peaks and their intensities are listed in Table (1). Collagen type I exhibits a very strong peak at 3.23THz followed by a well resolved strong one at 3.35THz, Fig.1 (i-a). It also shows some weak broad peaks located at 2.71, 2.86, doublet at 2.94 and 2.99, and broad shoulder at 3.13THz.

In the region lower than 2.6THz, cortex exhibits some absorption peaks with different intensities, Fig.1 (i-b). In the region higher than 2.6THz, it demonstrates some close similarities and some differences in the spectral pattern compared to those of collagen. This result recommends that the cortex sample still contain some residual organic material, a matter to be confirmed by the conventional FT-IR method.

Our goal is to differentiate between normal and demineralized bone based on the THz response for biological applications. To the best of our knowledge, we are the first to inspect the DBM using the THz waves. The characteristic absorption features of normal and DBM of camel cranial and femur in the range 0.06-3.5THz measured by TPS are shown in Fig. 1(ii) and (iii), respectively. The recorded peak frequencies and their intensities are listed in Table (2). Apart from the reduced intensity of the absorption peaks, the THz absorption spectra of the demineralized cranial bone, Fig. 1(ii), shows similar pattern to that of the control bone in the range of 1.75-3.5THz. Characteristic vibration modes are seen in the range 0.5-1.75THz. The normal cranial bone illustrates a very strong sharp peak at 0.73 THz and strong broad one at 1.57 THz with a strong broad shoulder at its left side at about 1.38 THz. On the other hand, DBM presents a very strong broad band at 0.81 THz with two little humps at about 1.29 and 1.46THz.

Regarding the demineralization effect on the camel femoral bone, Fig. 1(iii), both THz spectra of control and DBM have common and similar

TABLE (1): The quantitative degree of demineralization (in %) of camel femur and cranial due to HCl-treatment as measured by the ash content.

Sample	Control	HCl-treated	%D.D
Femur	**64.09**	**54**	**15.74%**
Cranial	79.51	70.22	**11.68%**

TABLE (2): Calcium/Phosphate ratio of camel femur and cranial measured by ICP and the indicated mineral type.

Sample	Ca/P ratio	Mineral	Symbol	Reference
Femur Control	**1.244**	**Amorphous calcium phosphate**	**ACP**	***Zhao et al., 2011***
Femur HCl-treated	**0.903**	**Brushite (dibasic calcium phosphate dehydrate)**	**DCPD**	***Mekmene et al., 2009***
Cranial Control	**1.270**	**Octacalcium phosphate**	**OCP**	***LeGeros 1991***
Cranial HCl-treated	**1.094**	**Monetite [Dicalcium phosphate]**	**DCP**	***Habraken et al., 2016***

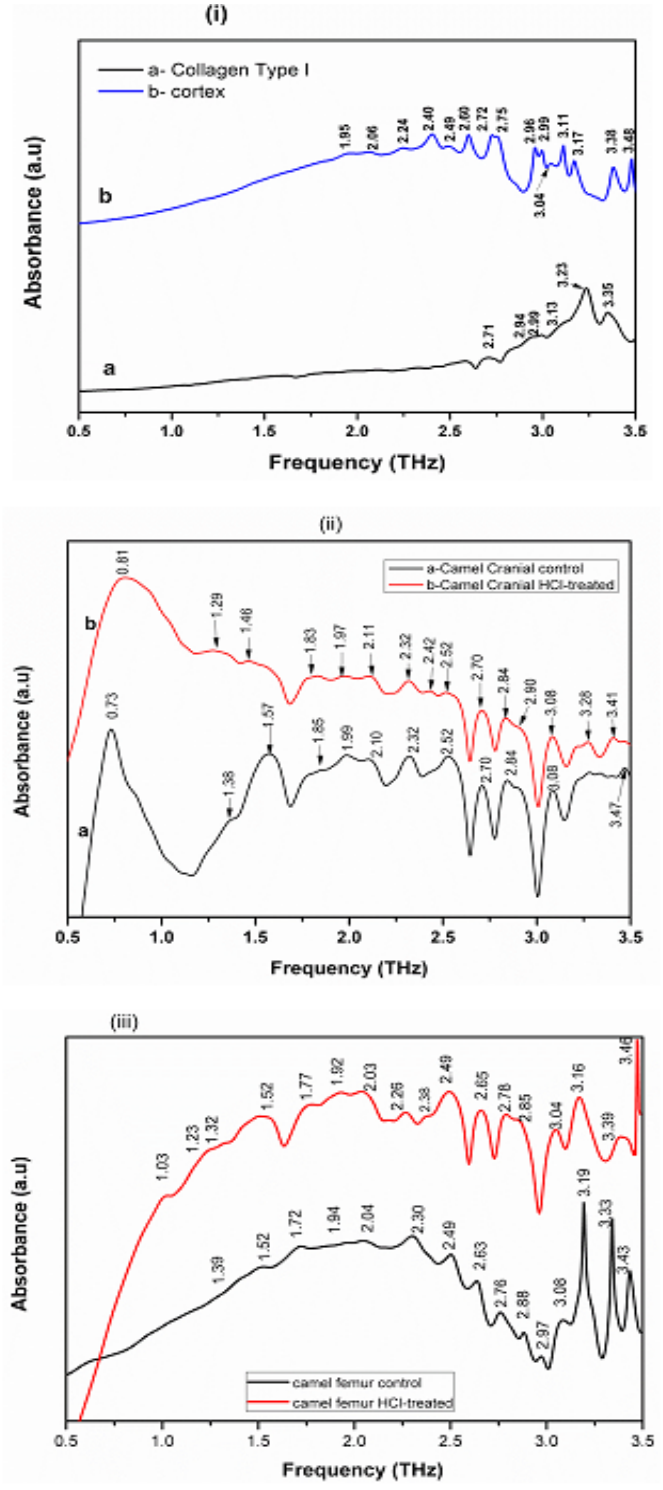

Fig. 1. Terahertz absorption spectra of (i) collagen type I, natural hydroxyapatite (cortex), (ii) normal and demineralized camel cranial bone, and (iii) normal and demineralized camel femoral bone

absorption humps up to nearly 2THz. Careful examination of the two spectra, over the range 2-3.5THz, revealed close correlation between the demineralization process and the spectral features. There are some unique vibrations modes of the control femur bone (a) occur at 2.30, 2.97 and 3.33THz, and disappeared as the result of demineralization. Furthermore, the spectral pattern of the normal bone is characterized by strongly descending intensity of sharp peaks at 3.19, 3.33, and 3.43THz in addition to a group of medium intensity well resolved peaks at 2.30, 2.49, 2.63, 2.76, 2.88, 2.97, and 3.08THz, respectively. However, the femoral DBM (b) is recognized by its strong and smooth spectral features with some frequency shift from those of the normal femur. Moreover, it demonstrates two new broad peaks of weak intensity at 2.26 and 2.38THz.

Owing to the fast recent development in THz spectroscopy, many chemical compounds and biomolecules can give a specific "fingerprint" of their molecular substance. This is significant to the intramolecular, and intermolecular modes arising from the hydrogen-bonding interaction, van der Waals force and other weak interactions [22]. Markelz et al. (2000) had the forefront of using pulsed terahertz spectroscopy to examine the low-frequency collective vibrational modes of biomolecules[12]. Their results revealed increment in the broadband absorption with the frequency of lyophilized powders of calf thymus DNA, bovine serum albumin and collagen in the 0.06-2.00 THz frequency range in a manner of Beer's law behavior. Particularly, collagen exhibited rapid absorbance increase with increasing frequency. They proposed that a large number of the low-frequency collective modes for these systems are infrared active. Although, our results of collagen were obtained in a frequency range higher than their range but agree with theirs taking into consideration the appearance of strong peaks at higher frequencies (2.5-3 .5THz).

Corridon and Wilke (2007) measured the change of some THz properties in collagen hydrated in different concentrations of saline during 24 hours dehydration period [23] . Mizuno et al. (2014) measured the absorption response of collagen from different sources to the THz radiation in the frequency range 100-600 cm^{-1} (3-18THz) after being exposed to pure water and phosphate buffer solution (PBS) [8]. They recorded two peaks at 340 and 540 cm^{-1} for the collagen penetrated by pure water, while that penetrated by PBS showed new distinctive peak at 168cm^{-1}. They pointed out that all collagen kinds gave the same absorption spectra, in spite of their different amino acid compositions, assuming that the absorption in that frequency range is mainly due to the glycine which is common in the central helical axis of the collagen [8]. They concluded that collagen fibers contraction and condensation can be easily detected by THz spectroscopy. Those works were done in a very different, frequency range higher than our measuring range, which makes it difficult to compare our results with theirs. Hence, we are the first reporting characteristic THz absorption peaks of collagen, normal bone powder, and DBM in the frequency range of 0.5-3.5THz.

The THz absorption spectra of the bone tissues obtained in the present study are comparable to those represented by Nikoghosyan et al. 2017 in the 0.2-2THz spectral range revealing several absorption lines beyond 1.6THz for the human jaw bone, and at 1.7THz for Cerabone bone substitute [24] . Plazanet et al. 2018 reported THz spectra of bovine femur bone, and commercial ns-HA powders when heated at ≥ 800°C, showing only one narrow peak at 2.1THz (equivalent to 2.8THz when compared to the DFT–simulated spectra), and attributed it to a lattice mode of stoichiometric HA [25]forensic and archaeological contexts, new investigation techniques are constantly required to better characterize bone ultrastructure. In the present paper, we provide an extended investigation of the vibrational features of bone tissue in the 0.1-3 THz frequency range by time-domain THz spectroscopy. Their assignment is supported by a combination of X-ray diffraction and DFT-normal modes calculations. We investigate the effect of heating on bone tissue and synthetic calcium-phosphates compounds with close structure and composition to bone mineral, including stoichiometric and non-stoichiometric hydroxyapatite (HA. Meanwhile, they demonstrated broad bands for some compounds (α- and β-TCP, β-CPP, TTCP and s-HA) that may be found in the heated bone. Although we neither heated nor DFT calculated our samples, all THz spectra of the cortex bone powder, cranial and femur control bones and their DBM showed vibrational modes around 2 and 2.8THz with different intensities and broadness which are supported by the findings of Plazanet et al. 2018 who also attributed the broadness of the modes to the crystalline defects. The number of the vibrational modes increases as the number

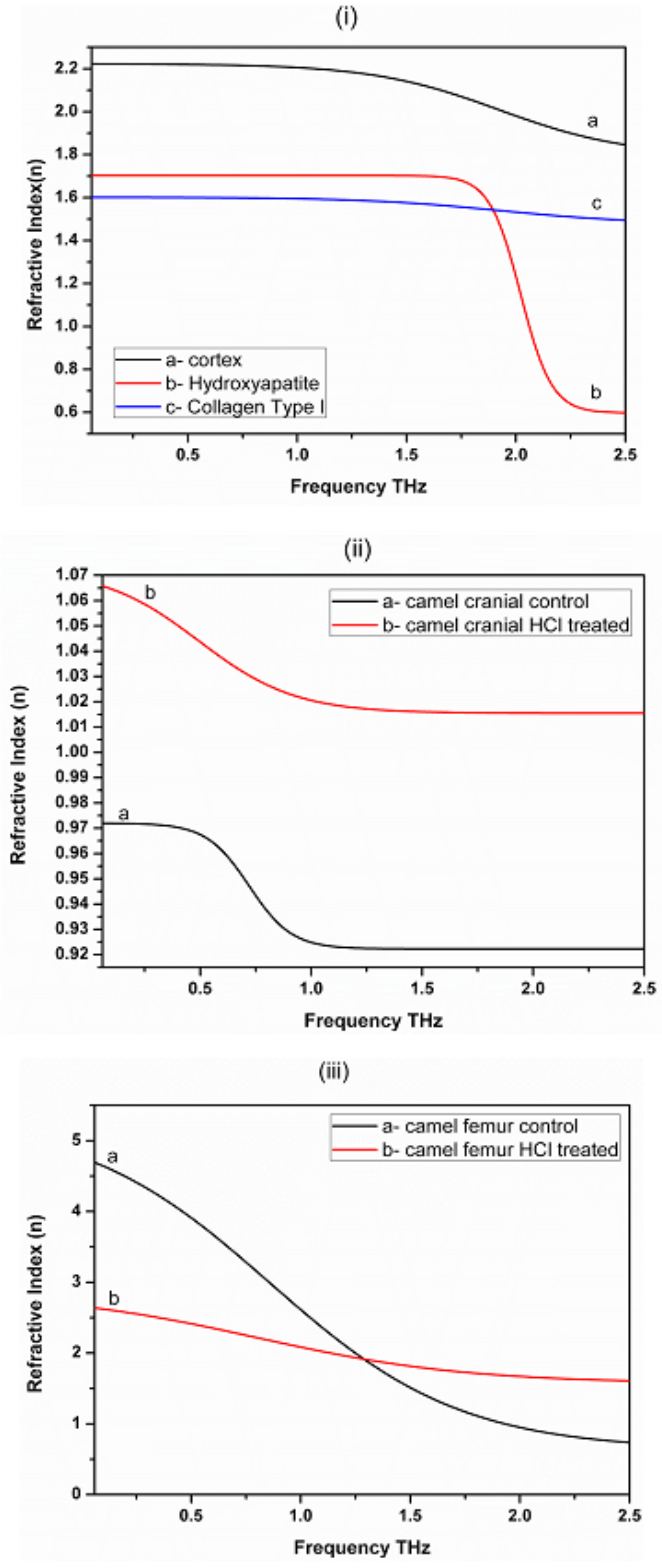

Fig. 2. Refractive indices of (i) collagen type I, synthetic and natural hydroxyapatite (cortex), (ii) normal and demineralized camel cranial bone, and (iii) normal and demineralized camel femoral bo

of atoms per unit cell increases, this fact can explain the presence of several broad resonance absorptions in our bone samples suggesting different phases with some degree of disorder.

Refractive Index (R.I)

Figure (2) illustrates the refractive indices of all examined materials in the range of 0.06-2.5THz. Over the entire range, cortex (i-a) always shows the maximum R.I. values. The natural and synthetic HA, and collagen exhibit nearly constant R.I with frequency up to 1.5 THz. The average values of the R.I of the cortical bone, HA, and collagen are 2.19±0.05, 1.70±0.002, and 1.59±0.002, respectively. After 1.5 THz and up to 2.5 THz, the cortex and collagen undergo slight gradual decrease in their R.I although, the synthetic HA shows sharp decline in its R.I.

The measured indices of refraction at particular frequencies, 0.5, 1, 1.5, and 2THz for the studied materials were investigated carefully. The HCl-treatment affected both cranial, and femur bone remarkably. R.I of the treated cranial bone increased by 7.87%, 10.36%, 10.16%, and 10.97% compared to the control at 0.5, 1, 1.5, and 2THz, respectively. The treated femur bone showed significant reduction rate in the R.I by 38.17%, and 18.93% at 0.5, and 1THz, respectively. Then, it reversed its trend remarkably giving a rate of increase 19.18%, and 76.86% at 1.5, and 2THz, respectively.

Berry et al. (2003) used a Pulsed Terahertz Imaging (PTI) system with a bandwidth of 0.5-2.5THz to establish a catalogue for the optical properties of human tissues such as cortical bone, tooth enamel and dentine, artery, vein, nerve, and skin adipose tissue. Refractive indices ranged from 1.5 ± 0.5 for adipose tissue, to 2.49± 0.07 for human cortical bone, 2.57±0.05 for tooth dentin, and 3.06 ± 0.09 for tooth enamel [26]"IS SN":"0277786X","PMID":"3800","abstract":" The first demonstrations of terahertz imaging in biomedicine were made several years ago, but few data are available on the optical properties of human tissue at terahertz frequencies. A catalogue of these properties has been established to estimate variability and determine the practicality of proposed medical applications in terms of penetration depth, image contrast and reflection at boundaries. A pulsed terahertz imaging system with a useful bandwidth 0.5-2.5 THz was used. Local ethical committee approval was obtained. Transmission measurements were made through tissue slices of thickness 0.08 to 1 mm, including tooth enamel and dentine, cortical bone, skin, adipose tissue and striated muscle. The mean and standard deviation for refractive index and linear attenuation coefficient, both broadband and as a function of frequency, were calculated. The measurements were used in simple models of the transmission, reflection and propagation of terahertz radiation in potential medical applications. Refractive indices ranged from 1.5 0.5 for adipose tissue to 3.06 0.09 for tooth enamel. Significant differences (P < 0.05

The frequency-dependent refractive index of human cortical bone was first investigated by Stringer et al. 2005 in the range 0.1-1.25THz [27]derived from human femur, have been studied using terahertz time-domain transmission spectroscopy. The relationship between the broadband THz parameters and the previously acquired values of Young's modulus and x-ray attenuation (CT number. They found evidence that the hydration level of the bone plays a key role in determining the THz parameters such as transmission and R.I. They recorded refractive indices 2.49 and 2.32 extracted from the time-domain results for ambient and forced dried cortical bone, respectively. Moreover, the frequency-domain calculations produced 2.36 R.I for the forced dried bone.

Sim et al. (2009) measured the frequency-dependent characteristics of enamel and dentin of human tooth through THz-TDS, the refraction index of enamel was found to be superior than that of dentin [18]. Nazarov et al. (2008) reported refractive indices of 2.4 and 3.2 for tooth dentine and enamel, respectively [28]. It could be pointed out that the composition of the dentin is close to that of the cortical bone as the former contains about 68% HA and the latter contains about 65% HA of their constituents. Thus, our result of the average R.I over the frequency range of 0.5-1.5THz of the partially deproteinated bovine cortical bone (2.19±0.05), and camel femur control bone (2.66±1.18) are comparable with those mentioned above.

Lee et al. 2015 used the polarization-dependent TPS in the range 0.05-2 THz to study the collagen properties of the human scleral tissues [29]. While the normal tissue was polarization-dependent, the cross-linked tissue showed polarization-independent transmission properties. They attributed their results to the regular parallel fibrils

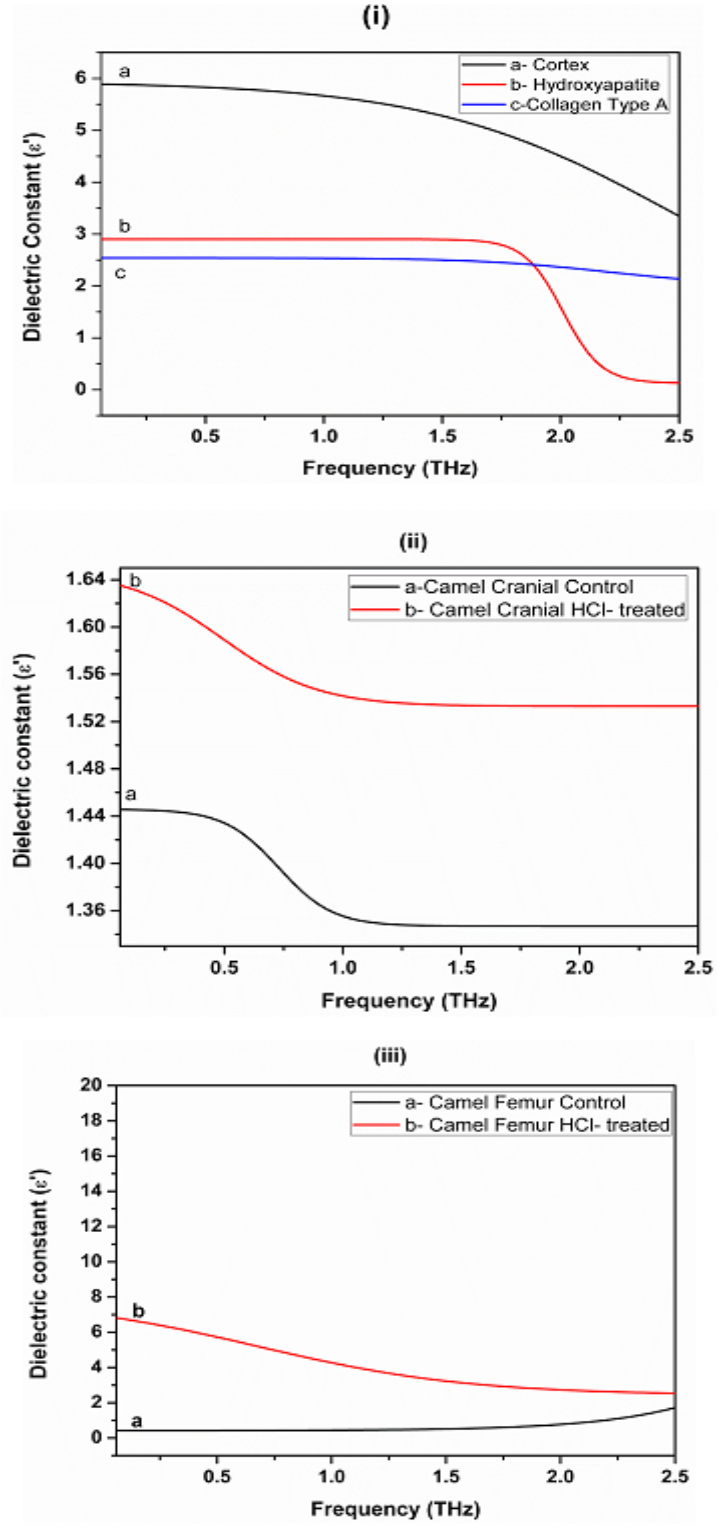

Fig. 3. Variation of the dielectric constant with THz frequency applied for (i) collagen type I, synthetic and natural hydroxyapatite (cortex), (ii) normal and demineralized camel cranial bone, and (iii) normal and demineralized camel femoral bone

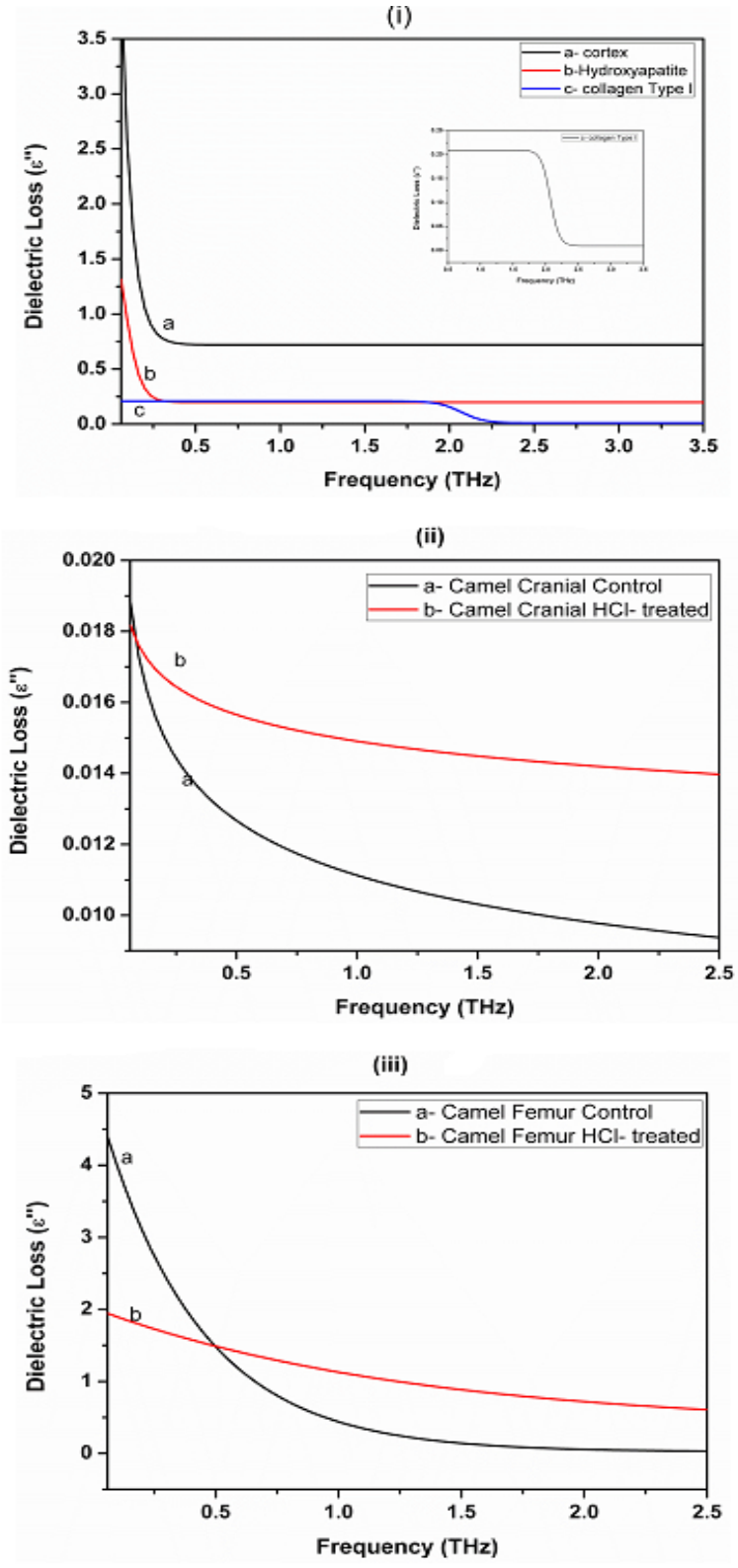

Fig. 4. Variation of the dielectric loss with THz frequency applied for (i) collagen type I, synthetic and natural hydroxyapatite (cortex), (ii) normal and demineralized camel cranial bone, and (iii) normal and demineralized camel femoral bone

arrangement of the former and interlocking fibrils arrangements of the latter. They found that the normal human scleral tissue was giving refractive index 1.5 corresponding to 168 μm sample thickness [29]. In the present study, the collagen type I recorded refractive index of (1.59±0.002) which is well correlated with that reported by Lee et al. 2015.

Therefore, THz refractive index is recommended to classify the different constituents of bone tissues for biological application, in consistence with Ashworth et al. (2009) who indicated that both THz pulsed spectroscopy (TPS) and THz Pulsed Imaging (TPI) can discriminate between healthy adipose, healthy fibrous and cancer breast tissue, through their complex refractive indices ranging from 0.15–2.0THz [14].

THz Dielectric Properties

A significant tool to recognize the material behavior is the dielectric measurement particularly at high frequencies because it can afford the magnetic or electrical characteristics of the materials. This is a serious parameter essential to implement the material in many applications. All materials are talented of storing electrical energy when they are exposed to an electric field. The storage capacity diverges from one material to another. Permittivity is a measure of the capability of a material to be polarized by an electric field. The electrode polarization is considered as a limiting factor in measuring the dielectric properties of biological tissues in a low frequency range, where the possible relaxation process can be shrouded [30]. Therefore, we employed the TPS to study the dielectric properties of the bone and its derivatives in such high terahertz frequency range. TPS uses coherent detection to measure the THz electric field, enabling information for both amplitude and phase of THz waves simultaneously. By applying the Fourier transformation on the gained waveforms, THz spectra will be obtained giving an opportunity to precise determination of refractive index (n) and absorption coefficient without applying Kramers-Kronig relations.

The real and imaginary parts of the dielectric permittivity of the bone components are measured in response to the THz exposure range from 0.06-2.5. Figures (3) and (4) show the dependence of the real dielectric permittivity constant (ε′), and the imaginary dielectric loss (ε″), respectively on the frequency as well as on the nature of the material. The naturally prepared HA (cortex) has much higher permittivity than either the synthetic HA or collagen (i). Demineralization via HCl-treatment of both cranial (ii) and femur (iii) bone produced remarkable increase in the permittivity values in comparison to the control bone.

In order to investigate these variations on quantitative basis, values of the dielectric permittivity and loss at fixed frequencies, namely 0.5, 1, 1.5, and 2THz, are calculated as average of three independent measures for all samples. Values of the έ of the cortex seem to be equal to the sum of those of HA and collagen. The ratio between $\varepsilon'_{cortex}/(\varepsilon'_{HA}+\varepsilon'_{collagen})$ was found to be 1.07, 1.04, 0.98, and 1.15 at 0.5, 1, 1.5, and 2THz, respectively. Moreover, values of the ε" of the cortex appear to be nearly doubled over the sum of those values of HA and collagen. The ratio between $\varepsilon''_{cortex}/(\varepsilon''_{HA}+\varepsilon''_{collagen})$ was found to be 1.76 at 0.5, 1, 1.5THz, and 2 at 2THz. Hence, it may be concluded that the naturally prepared hydroxyapatite contains some organic material and there is no interaction between the organic matrix and the inorganic hydroxyapatite in the bone. This result will be confirmed by the FT-IR.

Comparing the HCl-treated bone samples to their controls, the dielectric permittivity constant (ε′) increased by about 1.14 and 13-4 folds for cranial and femur, respectively. It could be mentioned that the rate of increase in ε′ of the demineralized femur bovine bones with respect to their control is descending order (13, 10, 6, 4 folds) with the rise in frequency (0.5, 1, 1.5, 2THz). The demineralized bones also exhibit a noticeable increase in the values of the dielectric loss (ε″) relative to their untreated samples. The treated cranial bones undertake increase in their ε″ values compared to their untreated samples by 1.24, 1.34, 1.42, and 1.46 folds at the frequencies 0.5, 1, 1.5, and 2THz, respectively. In contrast to the ε′ of the treated femur bones, the increasing rate in ε″ of the treated femur bone with respect to their control showed ascending trend (1, 2.57, 6.13, 11.28 folds) supplemented with increasing the frequency (0.5, 1, 1.5, 2THz).

Dielectric constant or relative permittivity is material property that measures the capability to store electric charge or electrostatic energy. Subsequently, it is a direct measure of the material polarizability in the presence of an electric field. Some researchers investigated the relationship between the electric properties of bone and

frequency, hydration levels, and measurement direction. El-Bassyouni et al. (2013) studied the dielectric properties of dog cranial bone demineralized using different acids. They found that HCl demineralization reduced the calcium and phosphorus content by one third and one tenth of their control values, respectively yielding uppermost protein content. In contrast to our results, DBM THz dielectric parameters, they reported lower dielectric properties of DBM compared to the control in the frequency range 0.1-10 KHz, showing high dissipation of electric energy with more than one relaxation mechanism [19].

A recent work by Unal et al. (2018) studied the cross-property connections between the electrical and mechanical properties of wet and dehydrated bovine cortical bone in the frequency range 20Hz-2MHz [31]specific impedance, dielectric constant, and conductivity. Their results indicated a frequency-dependent trend of a linear relationship between the dielectric constant and the mechanical properties of bone, giving maximum correlation at 0.5MHz with toughness and elastic modulus. They suggested the measurement of electrical properties of cortical bone as a means for quantitative diagnosis of bone fracture resistance, since they represent about 57% of the variation in the cortical bone mechanical properties. They also reported that the ε of bone was significantly declined after removing of unbound and bound water components (200^{o}C and 400^{o}C heat treatment), but did not show more observable change after removal of the organic matrix (1000^{o}C heat treatment) at the entire frequency range. They also revealed the predominant contribution of the mineral-bound water on the electrical properties of bone compared with the effect of collagen-bound at high frequency (above 1MHz).

The recorded ε values of the dry synthetic pure HA showed minor values than the dry cortical bone powder after removing the organic compartment (dried at 100^{o}C) in the broadband range. This finding disagrees with that reported by Unal et al. 2018 [31]specific impedance, dielectric constant, and conductivity. Such result together with our derived result of $\acute{\varepsilon}_{cortex}$/ ($\acute{\varepsilon}_{HA}$+ $\acute{\varepsilon}_{collagen}$) confirm that the naturally prepared HA still contains some residues of the organic component, collagen-bound and mineral-bound water contributing in the permittivity. Herein, our results coincide well with those of Unal and his co-researchers, recommending the THz dielectric properties of bone as a sensitive predictor to the composition and microstructure of bone for different biological applications.

FT-IR spectroscopy

FT-IR spectroscopy is an outstanding tool characterizing the chemical composition of bone matrix (BM). It is a physicochemical, non-invasive technique used to measure the absorption of the infrared radiation from chemical bonds in the molecules functional groups. BM absorbs the infrared radiation at different, regions within the range of 400-4000 cm^{-1} in the spectrum of the hydroxyapatite [32]. However, there are few other bands (around 870 cm^{-1} and 1400-1450 cm^{-1}) initiated from carbonate substitutions in the crystal lattice of the hydroxyapatite. Bands assessed for collagen in the spectrum are at 1200-1700 cm^{-1} and 2800-3700 cm^{-1} regions, and those at 500-700 cm^{-1} are carbonate ions of substitute bone apatite.

Hydroxyapatite (Fig. 5b) is dominating as the most significant mineral phase in bone. The characteristic chemical groups are $PO4^{3-}$, OH^{-}, $CO3^{2-}$, as well as $HPO4^{2-}$ that characterize non-stoichiometric HA [33] The absorption band at 1022-1089 cm^{-1} is distinctive of the υ_3 $PO4^{3-}$ asymmetric stretching [34] as well as the bands at 560 and 600 cm^{-1} assigned for υ_4PO4^{3-} bending vibration and at 961 cm^{-1} typical of υ_1 $PO4^{3-}$ symmetric stretching [35]. Cortex (Fig. 5c) shows a broad band in the range of 3550-2950 cm^{-1}, assigned for O-H stretching of Amide A proteins. The small bands at 2927 and 2858 cm^{-1} are assigned for asymmetric and symmetric C-H stretching of CH_2. The band at 1030 cm^{-1} could be assigned to υ_3 $PO4^{3-}$ asymmetric stretching of phosphate. The PO_4 structural units were characterized by the ν_3 antisymmetric stretching (P-O) vibrational mode [36]. Collagen (Fig. 5a) showed the following bands: 1633 cm^{-1} (C=O) corresponding to Amide I, 1550 cm^{-1} corresponding to Amide II δ(NH) + υ(CN), most bands above 1500 cm^{-1} are assigned to vibrations from the amide groups from collagen. The band at 3280 cm^{-1} conforming Amide A (N-H), the peaks at 2956 cm^{-1} matching to functional group CH_3, 2924cm^{-1} to CH_2, 1250cm^{-1} to Amide III δ(NH) + υ(CN), and 3070 cm^{-1} to Amide B (CH_2) can be seen. Those functional groups are corresponding to the collagen matrix [37].

Fig. (6-i) demonstrates the FT-IR absorption bands of cranial bone, they are typically assigned to carbonate, phosphate and some organic groups.

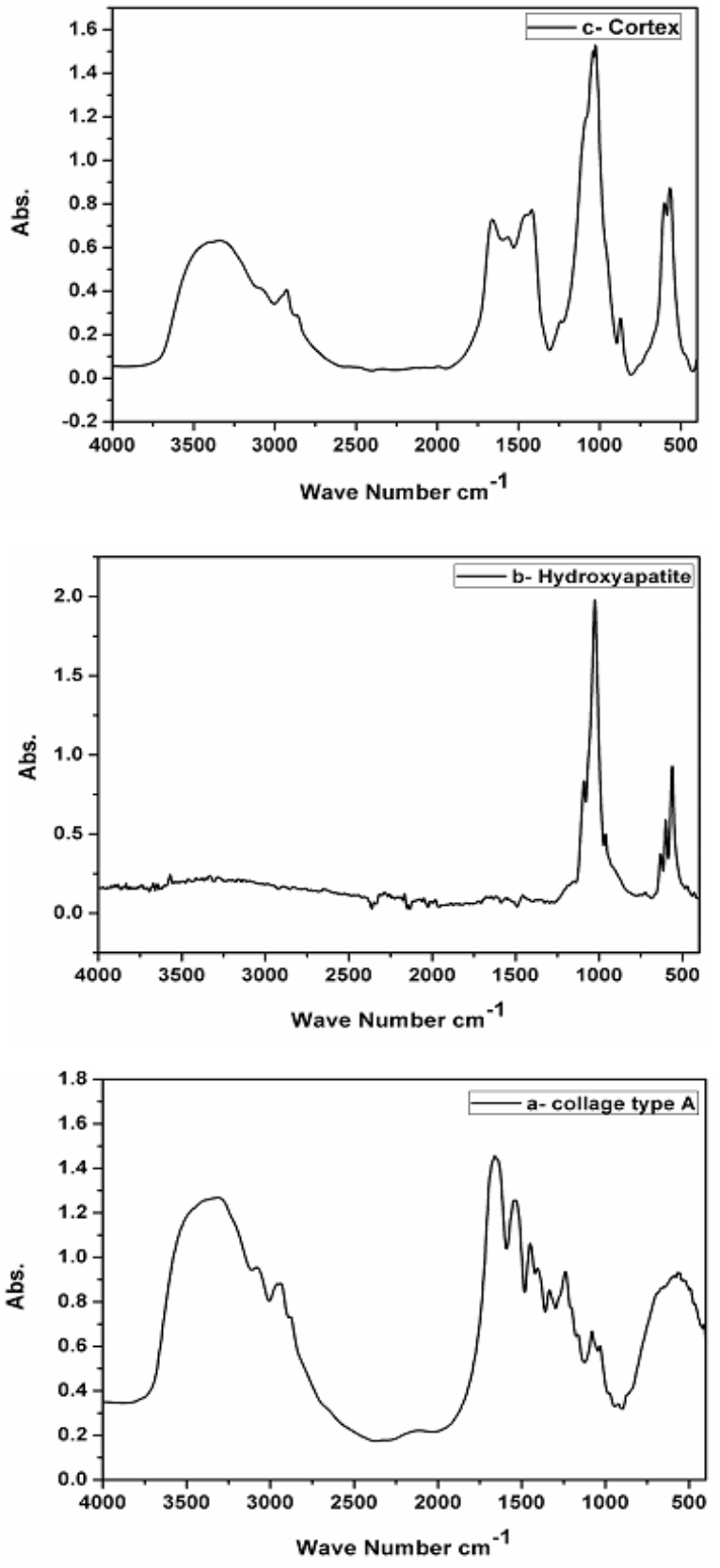

Fig. 5: FT-IR absorption spectra of (a) collagen type I, (b) HA and (c) cortex

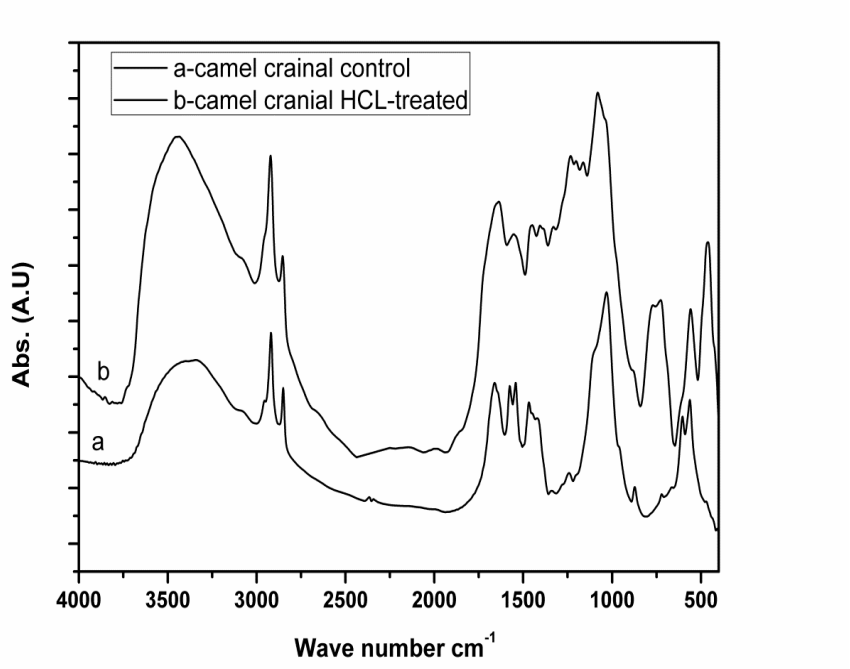

Fig. 6-i: FT-IR absorption spectra of (a) camel cranial control and (b) camel cranial HCl-treated

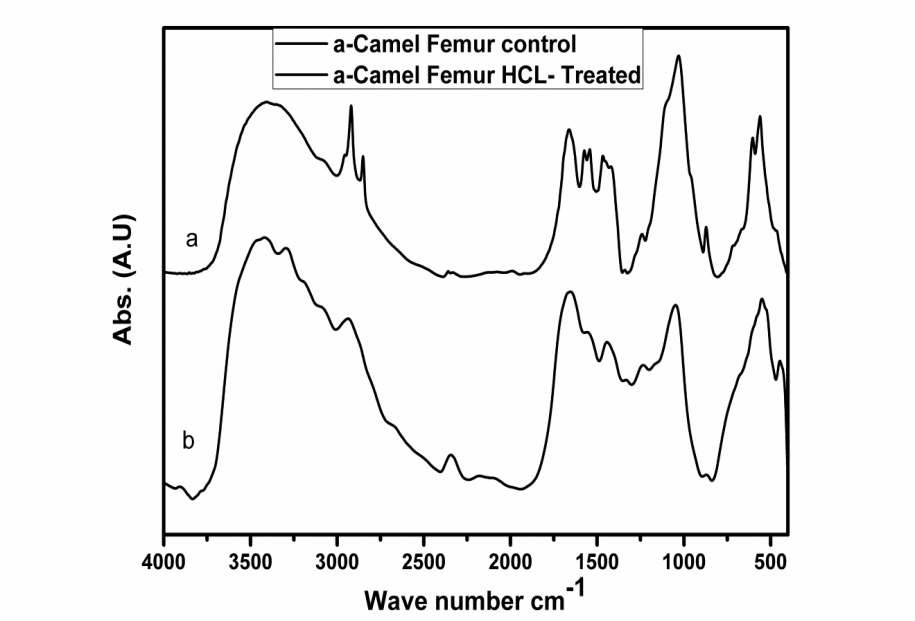

Fig. 6-ii: FT-IR absorbance spectra of (a) Camel femur control, (b) Camel femur HCl- treated

The most intense FT-IR feature is the broad strong absorption band at 1200-900 cm^{-1}, which is assigned to the ν_1 and ν_3 normal vibrational modes of phosphate ions (PO_4^{3-}). The two bands in the 650-500 cm^{-1} spectral region mainly originate from the ν4 bending mode of PO_4^{3-} [38]. Those bands are mainly due to the hydroxyapatite present in the inorganic portion of bone. In the 1600-1300 cm^{-1} range, bands due to the stretching modes of carbonate ions (CO_3^{2-}) are visible, and partially overlap with the bands of amide II. Bands in this region are significance of some hydroxyapatite anions being replaced by carbonate [39]especially in dental applications. In such cases, bone regeneration and new bone quality can determine the success of the treatment. This study investigated the main spectral differences of undamaged and healed bone using the ATR-FTIR spectroscopy technique. Three rabbits were submitted to a surgical procedure; a small piece of bone (3×3 mm 2.

An important biological band spectra is the Amide I band that arises from coupled ν C=O stretching and N-H bending of proteins at 1635 cm^{-1}, it is subtle to changes in protein secondary structure [40]and thus extension of Depciuch et al. research studies (2016. Other representative peaks of protein occur at different wavenumbers: **(1)** band at 1162cm^{-1} corresponding to ν C-O stretching mode of C-OH groups of protein, **(2)** at 1234cm^{-1} corresponds to Amide III (δ N-H bending, ν C-N stretching, ν C-C stretching) – protein [41], **(3)** at 1462cm^{-1} due to δ CH_2 scissoring vibrations mode was observed **(4)** band at 1540cm^{-1} agrees to Amide II (δ N-H bending and ν C-N stretching) - protein, **(5)** at 3283cm^{-1} corresponding to υNH stretching of the peptide bond (-NHCO-) of proteins and υOH stretching of functional groups of water.

FT-IR analyzed the consequent changes in the chemical composition of the cranial demineralized bone. Higher intensity was detected in demineralized sample compared to the control. This might be attributed to the increase in vibration of the different functional groups upon demineralization [32]. A peak at 870cm^{-1} indicates the carbonate replacement in the resulting apatite and a double band in the range of 1370-1450cm^{-1} indicating the CH2 [42]combining both osteoconductive and osteoinductive properties, conflicting results have been published in the literature regarding its bone-inducing abilities. This may be a consequence of following different demineralization procedures that naturally result in products with different properties.The present work examines the evaluation of the demineralization process of similar samples of human cortical bone using three different concentrations of hydrochloric acid solutions (0.6. M, 1.2. M and 2.4. M. The appearance of new peaks are consistent to collagen which displayed that demineralization impacted the camel bone and released calcium, thus affluence vibration of the molecules, especially the proteins [43]. These findings are in consistent with the newly detected peaks in the THz spectrum.

IR spectra of both (a) camel femur control and (b) the HCl-treated bone are represented in Fig. (6-ii)**.** Most intense bands in the spectrum are of hydroxyapatite at (500-700cm^{-1}) and (900-1200cm^{-1}) and that of collagen in the range of (1200-1700cm^{-1}) and (2800-3700cm^{-1}). After HCl treatment, FT-IR monitored consequent changes in their chemical composition. The bands at 561 and 603cm^{-1} correspond mainly to $\upsilon_4PO_4^{3-}$ bending vibrations, despite some minor influence from collagen (amide bands) in that region. The band at 960cm^{-1} was assigned to υ_1P-O symmetric stretching mode. The strong band at 1032cm^{-1} and shoulder at 1242cm^{-1} could be assigned to $\upsilon_3PO_4^{3-}$ asymmetric stretching of phosphate. The bands assigned for both stretching and bending mode of vibration of PO_4^{3-} confirmed the presence of the β-tricalcium phosphate (β-TCP). The splitting of the band around 600cm^{-1} symbolized the presence of hydroxyapatite (HA) [44]. The band at 872cm^{-1} was characteristic of carbonate bending vibration substituted for PO_4^3. Alternatively, the collagen moiety of bone originates at the typical Amide I and Amide II bands at 1634 and 1548cm^{-1}, respectively. Most bands above 1500cm^{-1} were assigned to vibrations from the amide groups from collagen [45]. Three bands in the range of 1420-1574cm^{-1} assigned to $\upsilon_3CO_3^{2-}$ stretching vibration mode also approved the substitution of B-type [46]. The broad band at about 3412cm^{-1} was assigned to the O-H stretching mode [47]. The band at 1660cm^{-1} could be assigned to a combination of the H-bonding of H_2O molecules and proteins (amide groups of organic matrix). The intensity of the demineralized femur was reduced compared to control. These results designated that the HCl has minor crystalline changes in case of camel femur bone.

Degree of Demineralization

The percentage degree of demineralization

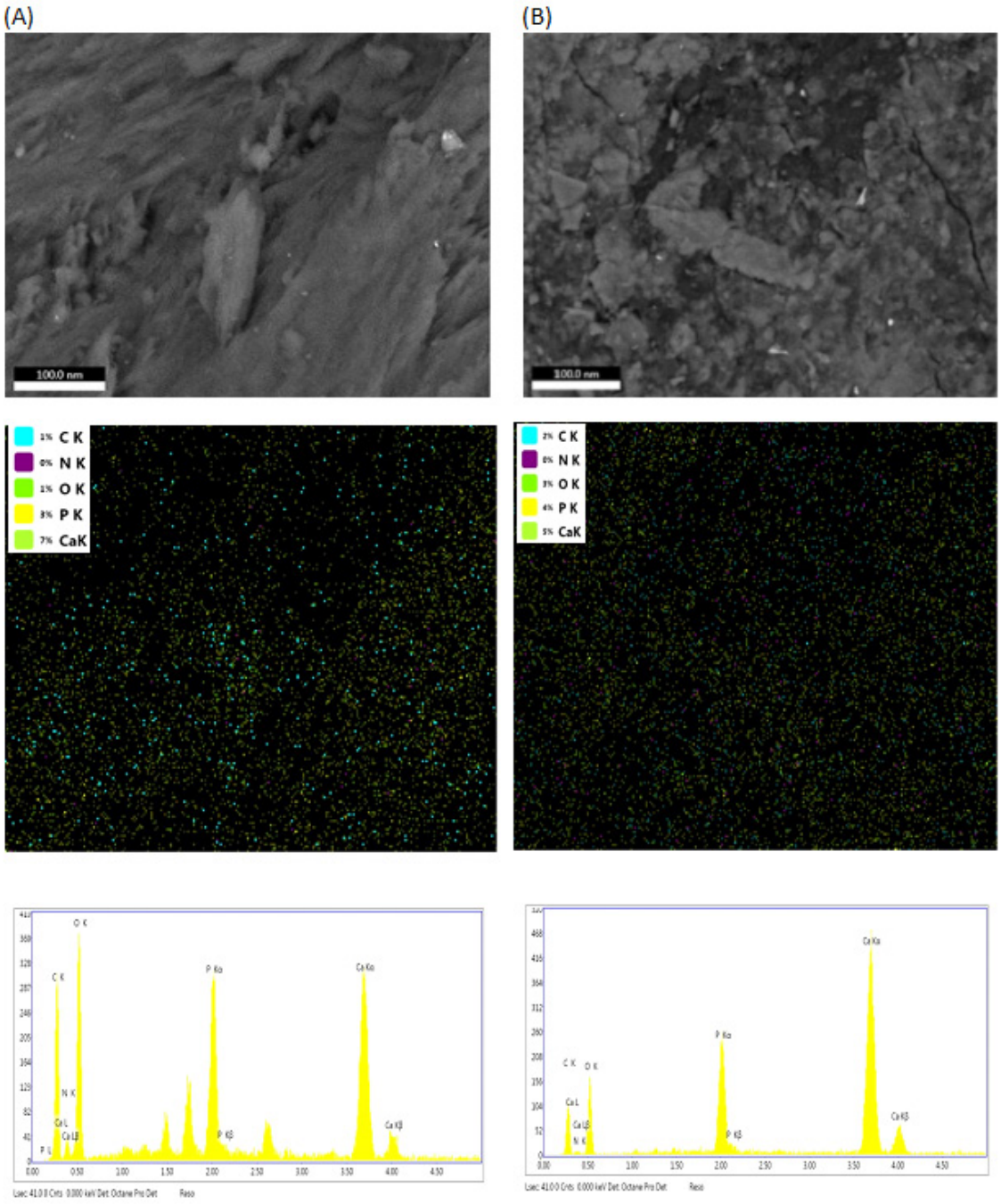

Fig. 7. EDX mapping for Camel Femur control (A) and HCl Treated (B).

Top of Form

(%D.D), Ca/P ratios, morphological changes and elemental distribution were assessed by the well-established conventional techniques for two reasons. The first was to detect the mineral reduction produced by the HCl treatment, and the second was to compare and support the new findings obtained by TDS. Results of the ash content (Table 1) show that the cranial control bones have higher mineral content compared with that of the femur control, and the extent of demineralization is higher in case of femur (15.74%) than in that of cranial (11.68%) bones. Ca/P ratios shown in Table 2 reflect the mineral reduction and its consequent phase assignements [48–51], which come to an agreement with the %D.D. Also SEM images reveal the difference between the control and demineralized bone, and EDX mapping shows the elemental distribution before and after treatment (Figure 7). Moreover, the different phases of the bone minerals listed in Table 2 besides the elemental distribution (produced as a result of the partial demineralization process) can explain the several resonance absorptions obtained in the THz-TDS spectra. The results of Ca/P ratio and %D.D of the cranial and femoral DBM can elucidate the increase in the optical and dielectric properties attributing this increase to the amount of minerals lost.

Conclusions

In this work, we succeeded to distinguish between different types of bone and their demineralized forms based on their THz response. We can summarize our conclusions in the following points:

1- THz absorption fingerprint was recorded for each bone compartment (mineral/collagen), type (cranial/femur), and DBM.

2- THz absorption spectra of the natural HA were sensitive enough to reveal the residual organic components, which were additionally confirmed by the FT-IR analysis.

3- Refractive indices of materials were frequency dependent on the THz range providing that the natural HA has the highest R.I values, 2.19±0.05 in the frequency range 0.06-1.5THz.

4- HCl treatment of bones (mineral loss) caused elevation in the values of the optical and dielectric properties with increasing frequency.

5- Femur DBM gave maximum rate of increase in R.I (about 77%) at 2THz relative to its control, which is much higher than that of cranial DBM (11%). Such result can be correlated to the %D.D which was higher for the femur DBM (15.74%) than the cranial DBM (11.68%).

6- Comprehensive qualitative and quantitative investigations of the THz dielectric properties demonstrated that έ, and ε” values of the natural HA were almost equivalent to, and double the straightforward sum of those values of synthetic HA and collagen, respectively. This finding is supported by the FT-IR results that proved the presence of residual collagen in the natural HA obtained from cortex.

7- Dielectric permittivity and loss constant were highly affected by the demineralization process giving rise to significant increase in έ and ε” values compared to their controls.

8- Cranial DBM recorded nearly constant rate of increase in έ values (1.14 folds), and ascending rate of increase in ε” values with increasing frequency (the maximum value 1.46 folds at 2 THz).

9- Femoral DBM similarly recorded remarkable increase in their έ values compared to their control at any frequency giving maximum and minimum rates of increase 13 folds and 4 folds at 0.5THz and 2THz, respectively. On the other hand, the ε” values were dramatically increasing with frequency in an ascending manner giving minimum and maximum rates of increase 2.57 folds and 11.28 folds at 1 THz and 2 THz, respectively.

10- The dramatic increase in both optical and dielectric properties of the DBM compared to the control in general, and in femoral DBM compared to the cranial DBM especially give the evidence that the %D.D and the consequent phase change play the key role in determining these vital properties.

11- TDS is a non-invasive technique that can throw new light on the spectral features and dielectric properties of different bone types and compartments and represents an effective tool study changes in the extracellular matrix.

Acknowledgment

The authors would like to thank Prof. Azza Ward, professor of physics at Microwave Physics and Dielectrics Department, National Research Centre, Egypt for her advice and revision of the dielectric part in this study. This research did not receive any specific grant from funding agencies in public, commercial, or not-for-profit sector.

Contributors

SKHK and GTE conceived, designed, and performed the experiments. WME performed the technical measurements. SKHK and WME processed the data and did the calculations. SKHK, WME, and GTE wrote the manuscript. All authors have approved the final article.

Conflicts of interest

The authors declare that there is no conflict of interest

References

1. Saini, K., Discher, D., Kumar, N. Static and time-dependent mechanical response of organic matrix of bone. *J Mech Behav Biomed Mater*, **91**, 315 (2019).

2. Roschger, P., Fratzl-Zelman, N., Misof, B.M., Glorieux, F.H., Klaushofer, K., Rauch, F. Evidence that abnormal high bone mineralization in growing children with osteogenesis imperfecta is not associated with specific collagen mutations. *Calcif Tissue Int*, **82**, 263 (2008).

3. Ruffoni, D., Fratzl, P., Roschger, P., Klaushofer, K., Weinkamer, R. The bone mineralization density distribution as a fingerprint of the mineralization process. *Bone*, **40**, 1308 (2007).

4. Gruskin, E., Doll, B.A., Futrell, F.W., Schmitz, J.P., Hollinger, J.O. Demineralized bone matrix in bone repair: History and use. *Adv Drug Deliv Rev*, **64**, 1063 (2012).

5. De La Vega, R.E., De Padilla, C.L., Trujillo, M., Quirk, N., Porter, R.M., Evans, C.H., Ferreira, E. Contribution of Implanted, Genetically Modified Muscle Progenitor Cells Expressing BMP-2 to New Bone Formation in a Rat Osseous Defect. *Mol Ther*, **26**, 208 (2018)

6. Unal, M., Yang, S., Akkus, O. Molecular spectroscopic identification of the water compartments in bone. *Bone*, **67**, 228 (2014).

7. Zhang, W., Chen, J., Tao, J., Jiang, Y., Hu, C., Huang, L., Ji, J., Ouyang, H.W. The use of type 1 collagen scaffold containing stromal cell-derived factor-1 to create a matrix environment conducive to partial-thickness cartilage defects repair. *Biomaterials*, **34**, 713 (2013).

8. Mizuno, M., Yamada, A., Fukunaga, K., Kojima, H. Terahertz observation of salt penetration in collagen fibers. In Proceedings of the International Conference on Infrared, Millimeter, and Terahertz Waves, IRMMW-THz, 2014.

9. Mantsch, H.H., Naumann, D. Terahertz spectroscopy: The renaissance of far infrared spectroscopy. *J Mol Struct*, **964**, 1 (2010).

10. Yetimoglu NO, K.K. Applications of Terahertz Imaging in Medicine. *Omi J Radiol*, **03**, 7964. (2014)

11. Samanta, G., Mitra, D. Wideband THz antenna using graphene based tunable circular reactive impedance substrate. *Optik (Stuttg)*, **158**, 1080 (2018).

12. Markelz, A.., Roitberg, A., Heilweil, E.. Pulsed terahertz spectroscopy of DNA, bovine serum albumin and collagen between 0.1 and 2.0 THz. *Chem Phys Lett*, **320**, 42 (2000).

13. El Haddad, J., Bousquet, B., Canioni, L., Mounaix, P. Review in terahertz spectral analysis. *TrAC - Trends Anal Chem*, **44**, 98 (2013).

14. Ashworth, P.C., Pickwell-MacPherson, E., Provenzano, E., Pinder, S.E., Purushotham, A.D., Pepper, M., Wallace, V.P. Terahertz pulsed spectroscopy of freshly excised human breast cancer. *Opt Express*, **17**, 124 (2009).

15. Chen, T., Li, Z., Mo, W. Identification of biomolecules by terahertz spectroscopy and fuzzy pattern recognition. *Spectrochim Acta - Part A Mol Biomol Spectrosc*, **106**, 48 (2013).

16. Cherkasova, O.P., M.Nazarov, M., Shkurinov, A.P., Fedorov, V.I. Terahertz spectroscopy of biological molecules. *Radiophys Quantum Electron*, **52**, 518 (2009).

17. Yin, M., Tang, S., Tong, M. The application of terahertz spectroscopy to liquid petrochemicals detection: A review. *Appl Spectrosc Rev*, **51**, 379 (2016).

18. Sim, Y.C., Maeng, I., Son, J.H. Frequency-dependent characteristics of terahertz radiation on the enamel and dentin of human tooth. *Curr Appl Phys*, **9**, 946 (2009).

19. El-Bassyouni, G.T., Guirguis, O.W., Abdel-Fattah, W.I. Morphological and macrostructural studies of dog cranial bone demineralized with different acids. *Curr Appl Phys*, **13**, 864 (2013).

20. Moharram, M.A., Khalil, S. Infrared study of

the interaction of acrylic bone cement with bone structurein vitro. *Int J Infrared Millimeter Waves*, **13**, 1217 (1992).

21. Moharram, M.A., Fadel, M.A., Higazy, H., Khalil, S. Interaction of Acrylic Bone Cement with Bone Structure. *Polym Plast Technol Eng*, **32**, 457 (1993).

22. Yan, H., Fan, W.H., Zheng, Z.P. Investigation on terahertz vibrational modes of crystalline benzoic acid. *Opt Commun*, **285**, 1593 (2012).

23. Corridon, P.M., Wilke, I. Monitoring the Dehydration of Collagen by Time-Domain Terahertz Transmission Measurements. *Cell* 1–2.

24. Nikoghosyan, A.S., Ting, H., Shen, J., Martirosyan, R.M., Kazaryan, M.A., Tunyan, M.Y., Papikyan, A. V., Papikyan, A.A. Dielectric Anisotropy of Human Bone and CERABONE® in the Terahertz Spectral Range 0.2 to 2.5 THz. In Proceedings of the Journal of Physics: Conference Series, (2017).

25. Plazanet, M., Tasseva, J., Bartolini, P., Taschin, A., Torre, R., Combes, C., Rey, C., Di Michele, A., Verezhak, M., Gourrier, A. Time-domain THz spectroscopy of the characteristics of hydroxyapatite provides a signature of heating in bone tissue. *PLoS One* (2018).

26. Berry, E., Fitzgerald, a J., Zinoviev, N.N., Walker, G.C., Homer-Vanniasinkam, S., Sudworth, C.D., Miles, R.E., Chamberlain, M., Smith, M. a Optical properties of tissue measured using terahertz-pulsed imaging. *Proc SPIE*, **5030**, 459 (2003).

27. Stringer, M.R., Lund, D.N., Foulds, A.P., Uddin, A., Berry, E., Miles, R.E., Davies, A.G. The analysis of human cortical bone by terahertz time-domain spectroscopy. *Phys Med Biol* (2005).

28. Nazarov, M.M., Shkurinov, A.P., Kuleshov, E.A., Tuchin, V. V Terahertz time-domain spectroscopy of biological tissues. *Quantum Electron*, **38**, 647 (2008).

29. Lee, J.W., Lee, Y.-S., Park, J.-M., Shin, D.-C., Jung, G.B., Shin, J.-H., Kim, S., Kee, C.-S., Kang, C. Terahertz spectroscopy of human sclera. *Curr Appl Phys*, **15**, 1156 (2015).

30. El-Hakam, R.A., Khalil, S., Mahani, R. Dielectric and FT-Raman spectroscopic approach to molecular identification of breast tumor tissues. *Spectrochim Acta - Part A Mol Biomol Spectrosc* **151**, 208 (2015).

31. Unal, M., Cingoz, F., Bagcioglu, C., Sozer, Y., Akkus, O. Interrelationships between electrical, mechanical and hydration properties of cortical bone. *J Mech Behav Biomed Mater*, **77**, 12 (2018)**.**

32. Figueiredo, M.M., Gamelas, J.A.F., Martins, A.G. Characterization of Bone and Bone-Based Graft Materials Using FTIR Spectroscopy. *Infrared Spectrosc - Life Biomed Sci* (2012).

33. Ratner An introduction to materials in medicine. *Biomater Sci*, **5**, 864 (2004).

34. Mobasherpour, I., Heshajin, M.S., Kazemzadeh, A., Zakeri, M. Synthesis of nanocrystalline hydroxyapatite by using precipitation method. *J Alloys Compd*, **430**, 330 (2007).

35. Ali, G.W., El-Hotaby, W., Hemdan, B., Abdel-Fattah, W.I. Thermosensitive chitosan/phosphate hydrogel-composites fortified with Ag versus Ag@Pd for biomedical applications. *Life Sci*, **194**, 185 (2018).

36. Grecu, R., Coman, V., Avram, V., Băciuţ, M., Băciuţ, G. Bone Matrices of Different Origins Studied by FTIR Spectroscopy. *Proc 1st Int Conf Adv Med Heal Care through Technol MediTech*, 429 (2007).

37. Sionkowska, A., Kozlowska, J. Characterization of collagen/hydroxyapatite composite sponges as a potential bone substitute. *Int J Biol Macromol*, **47**, 483 (2010).

38. 38. Liao, J.-G., Li, Y.-Q., Duan, X.-Z., Liu, Q. [Synthesis and characterization of CO-3(2-) doping nano-hydroxyapatite]. *Guang Pu Xue Yu Guang Pu Fen Xi*, **34**, 3011 (2014).

39. Benetti, C., Kazarain, S.G., Alves, M.A. V., Blay, A., Correa, L., Zezell, D.M. Attenuated total reflection Fourier transform infrared (ATR-FTIR) spectroscopic analysis of regenerated bone. *SPIE BiOS*, **8926**, 892641 (2014).

40. Chaber, R., Łach, K., Depciuch, J., Szmuc, K., Michalak, E., Raciborska, A., Koziorowska, A., Cebulski, J. Fourier Transform Infrared (FTIR) spectroscopy of paraffin and deparafinnized bone tissue samples as a diagnostic tool for Ewing sarcoma of bones. *Infrared Phys Technol*, **85**, 364 (2017).

41. Paschalis, E.P., Gamsjaeger, S., Klaushofer, K. Vibrational spectroscopic techniques to assess bone quality. *Osteoporos Int* 2017, **28**, 2275–2291.

42. Figueiredo, M., Cunha, S., Martins, G., Freitas, J., Judas, F., Figueiredo, H. Influence of hydrochloric acid concentration on the demineralization of cortical bone. *Chem Eng Res Des*, **89**, 116 (2011).

43. Novitskaya, E., Castro-Ceseña, A., Chen, P.Y., Vasquez, J., Urbaniak, R., Lee, S., Hirata, G., McKittrick, J. Investigations into demineralized cortical bone. In Proceedings of the Materials Research Society Symposium Proceedings, 1301,

33 (2011).

44. Berzina-Cimdina, L., Borodajenko, N. Research of Calcium Phosphates Using Fourier Transform Infrared Spectroscopy. In *Infrared Spectroscopy - Materials Science, Engineering and Technology*, ISBN 978-953-51-0537 (2012).

45. Murugan, R., Ramakrishna, S., Panduranga Rao, K. Nanoporous hydroxy-carbonate apatite scaffold made of natural bone. *Mater Lett*, **60**, 2844 (2006).

46. Fleet, M.E. Infrared spectra of carbonate apatites: ν2-Region bands. *Biomaterials*, **30**, 1473 (2009).

47. Wang, M., Qian, R., Bao, M., Gu, C., Zhu, P. Raman, FT-IR and XRD study of bovine bone mineral and carbonated apatites with different carbonate levels. *Mater Lett*, **210**, 203 (2018).

48. Zhao, J., Liu, Y., Sun, W. Bin, Zhang, H. Amorphous calcium phosphate and its application in dentistry. *Chem Cent J* , **5**, 40 (2011).

49. Mekmene, O., Quillard, S., Rouillon, T., Bouler, J.-M., Piot, M., Gaucheron, F. Effects of pH and Ca/P molar ratio on the quantity and crystalline structure of calcium phosphates obtained from aqueous solutions. *Dairy Sci Technol*, **89**, 301 (2009).

50. LeGeros, R.Z. Calcium phosphates in oral biology and medicine. *Monogr Oral Sci* (1991).

51. Habraken, W., Habibovic, P., Epple, M., Bohner, M. Calcium phosphates in biomedical applications: Materials for the future? *Mater Today,* **19***,* 69 (2016).